Nuclear reaction modeling of ^{52g}Mn production for multimodal imaging

A. Colombi(1)(2)(*), F. Barbaro(1)(3), L. Canton(3), M. P. Carante(2)
and A. Fontana(2)

(1) *Dipartimento di Fisica, Università di Pavia - Pavia, Italy*
(2) *INFN, Sezione di Pavia - Pavia, Italy*
(3) *INFN, Sezione di Padova - Padova, Italy*

Summary. — The present work is a theoretical investigation of nuclear reactions for the production of ^{52g}Mn that, with ^{51}Mn and ^{52m}Mn, is the only radionuclide that can be used for MultiModal Imaging PET-MRI. A comparison of different reactions is presented considering the reaction ^{nat}V(α,x)^{52g}Mn and the standard production routes with chromium targets. To optimize the production of the radionuclide of interest, an analysis of the cross sections is performed using three nuclear reaction codes (Talys, Fluka and Empire) to select the energy window corresponding to the maximum production of ^{52g}Mn and minimum of its contaminants. Numerical computations of the production rate and the time evolution of the produced nuclides are performed, leading to the calculation of the integral yield and of the isotopic and radionuclidic purities for each reaction. The result is that the reaction with ^{nat}V is very promising and competitive with the investigated standard production routes. Indeed, this reaction shows a radionuclidic purity high enough for clinical applications and an integral yield value even higher than that of the reaction with natural chromium target.

1. – Introduction

MultiModal Imaging (MMI) [1] is an emerging technique that consists in the combination of diagnostic exams based on different physical processes. It allows to obtain a single image with more detailed information about the organs of interest. Nowadays, different possibilities of MMI exist and are already available in clinics, like PET-CT [2], SPECT-CT [3], PET-MRI [4]. This study, in particular, is focused on the latter case

---

(*) Corresponding author. E-mail: alessandro.colombi@pv.infn.it

TABLE I. – *Comparison between properties of ^{52g}Mn and the principal radioisotope currently used in PET, ^{18}F.*

| Nuclide	$T_{1/2}$	$\langle E_{\beta+} \rangle$ keV	$I_{\beta+}$ %	Daughter
^{18}F	109.77 min	249.8	96.73	^{18}O
^{52g}Mn	5.591 d	241.59	29.4	^{52}Cr

that allows to obtain an image which shows morphological functional details (MRI) in addition to metabolic details (PET) [5].

At the moment PET-MRI imaging can be performed by scanning the patient sequentially (*i.e.*, the exams are taken separately) or simultaneously but, anyway, administrating two chemically different drugs to the patient [6]. In this work we consider production of ^{52g}Mn within the novel approach [7] of using one single radiopharmaceutical to perform both exams simultaneously.

With the use of ^{52g}Mn one has the advantage that the time required to perform the exams is shorter since they are done only in one step. ^{52g}Mn (with ^{51}Mn) is the only radionuclide that could be used for this purpose since it is paramagnetic and it has properties similar to ^{18}F, which is commonly used for PET. A comparison between these two isotopes is shown in table I. It is, therefore, interesting to investigate its production both theoretically and experimentally. This work represents the theoretical contribution to the INFN project METRICS (Multimodal pET/mRi Imaging with Cyclotron produced 51/52Mn and stable paramagnetic Mn iSotopes) of the INFN-LNL laboratories. At the moment, the standard production routes of ^{52g}Mn are based on the use of enriched and natural chromium targets

$$^{52}\text{Cr}(p,n)^{52g}\text{Mn}, \qquad ^{52}\text{Cr}(d,2n)^{52g}\text{Mn}, \qquad ^{nat}\text{Cr}(p,x)^{52g}\text{Mn}.$$
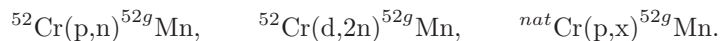
In this work we consider also the alternative reaction

$$^{nat}\text{V}(\alpha,x)^{52g}\text{Mn},$$
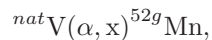
which is based on natural vanadium target and could represent a promising route.

A comparison of these reactions is performed in order to identify the best conditions for the production of ^{52g}Mn evaluating carefully the production of its contaminants. The integral yield and the purities are then calculated for each reaction.

2. – Methods

In each reaction several manganese nuclides are produced (their half-lives and decay properties are reported in table II) and the goal is to optimize the production of only ^{52g}Mn.

The study is initially based on the accurate analysis of the cross sections $\sigma(E)$ of each manganese nuclide. They are calculated using three nuclear reaction codes (Talys 1.9 [8], Empire 3.2 [9] and Fluka 2018.2.dev [10]). Talys allows to consider, for any reaction, combinations of different theoretical models. In particular we consider four

TABLE II. – *Physical characteristics of the radionuclides produced by the reactions under investigation.*

Radionuclide	Half-life	Decay mode	Mean energy (keV)
^{48}Mn	158.1 ms	$\beta^+/\beta^+,\mathrm{p}/\beta^+,\alpha$	6715.28
^{49}Mn	382 ms	β^+	6693
^{50g}Mn	283.29 ms	β^+	6611
^{50m}Mn	1.75 m	β^+	3515.43
^{51}Mn	46.2 m	β^+	2185.8
^{52g}Mn	5.591 d	β^+	575.84
^{52m}Mn	21.1 m	$\beta^+/$IT	2633.36
^{53}Mn	3.6×10^6 y	EC	597.00
^{54}Mn	312 d	EC$/\beta^-/\beta^+$	542.24
^{55}Mn	stable	–	–

models describing the preequilibrium mechanism and six models describing the level density [11,12]. The combinations of the models are analyzed and plotted with statistical descriptive tools: minimum, maximum, interquartile interval. For the latter, we calculate and use also its central value, that we indicate as *Best Theoretical Evaluation* (BTE), in order to identify a reference theoretical estimation of the considered quantities (for example of the integral yields). Also the Empire code is based on a variety of different models for the description of the nuclear reaction mechanisms, and in this work we consider the exciton model for the preequlibrium process. The Fluka code does not distinguish properly ground from metastable states as done by Talys and Empire and for this reason it is used only when this separation is not involved.

The analysis of the cross sections represents a preliminary study of the purity of the considered reaction, since it allows to identify the energy window corresponding to the maximum production of ^{52g}Mn and minimum of its contaminants. Among them only two nuclides (^{53}Mn and ^{54}Mn) have a half-life longer than that of ^{52g}Mn. In particular the former can be considered stable and, therefore, only the latter represents the main contaminant since it can affect the RadioNuclidic Purity (RNP) of ^{52g}Mn. For this reason it is important to compare the ^{52g}Mn and ^{54}Mn cross sections, and also to study their ratio

$$(1) \qquad r = \frac{\sigma_{52g\mathrm{Mn}}}{\sigma_{52g\mathrm{Mn}} + \sigma_{54\mathrm{Mn}}}.$$

The energy window selection is based on the maximum cross section position, for a larger production of ^{52g}Mn, with a ratio value close to 1 to maintain a low-contaminant production.

Once the energy window has been identified, we calculate numerically the production rate with the formula [13]

$$(2) \qquad R = \frac{I_0}{z_{proj}\,e} \frac{N_a}{A} \int_{E_{out}}^{E_{in}} \sigma(E) \left(\frac{\mathrm{d}E}{\rho_t \mathrm{d}x} \right)^{-1} \mathrm{d}E,$$

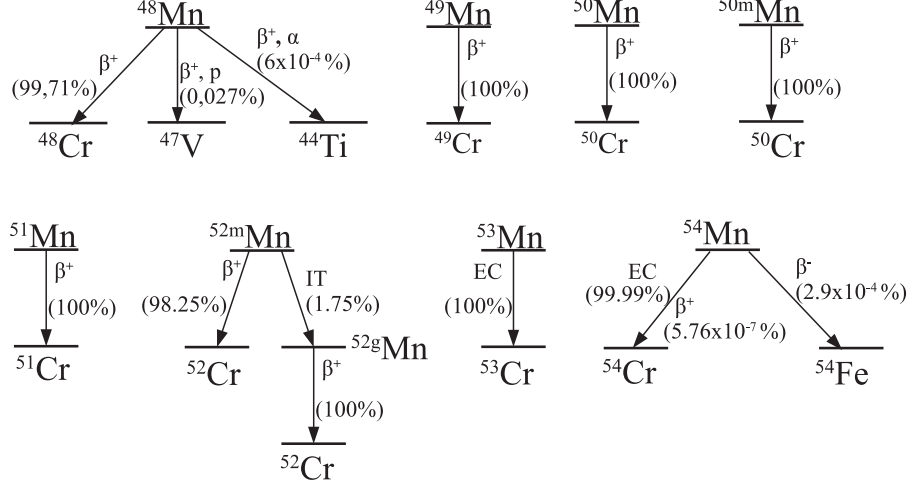where I_0 is the charge beam current, z_{proj} the atomic number of the incident particle, e

Fig. 1. – Decay schemes of the radioactive manganese nuclides produced in the reactions.

the electron charge, N_a the Avogadro number, A the target atomic mass, E_{in} and E_{out} the energy of the projectile impinging on the target and after exiting from the target, respectively, $\sigma(E)$ the production cross section for the nuclide, ρ_t the target density and dE/dx the stopping power of the projectile in the target, calculated with the Bethe-Bloch formula [14]. For each reaction we consider a target thickness of $200\,\mu$m and identical irradiation conditions ($I_0 = 1\,\mu$A and $t_{irrad} = 1$ h).

After this step, the decay schemes (fig. 1) and the half-lives of each nuclides are considered for the time evolution of the number of the produced nuclei $N(t)$ and their corresponding activities $A(t) = \lambda N(t)$. These two quantities allow to define the Isotopic Purity and the RadioNuclidic Purity. For example for the reaction with ^{nat}V for which the nuclides from ^{48}Mn to ^{55}Mn are produced

$$\text{(3a)} \qquad \text{IP}(t) = \frac{N_{^{52g}\text{Mn}}(t)}{N_{^{48}\text{Mn}}(t) + \cdots + N_{^{55}\text{Mn}}(t)},$$

$$\text{(3b)} \qquad \text{RNP}(t) = \frac{A_{^{52g}\text{Mn}}(t)}{A_{^{48}\text{Mn}}(t) + \cdots + A_{^{54}\text{Mn}}(t)}.$$

For each reaction we also calculate the integral yield representing the activity per unit of beam current per hour. This procedure allows to compare reactions with different projectiles and targets in order to identify the best production route with the RNP.

3. – Results

The procedure described in the previous section allows to select the energy windows for the optimal production of ^{52g}Mn for the different reactions and to obtain the purities and yields. The comparison of the cross sections between ^{52g}Mn and its contaminants is performed in fig. 2 where not only the cross sections are shown but also the ratio r (eq. (1)), with respect to the right vertical axis.

In ref. [15] the cross sections are represented in two different figures with all the available experimental data which are taken from the EXFOR database [16]. We refer to
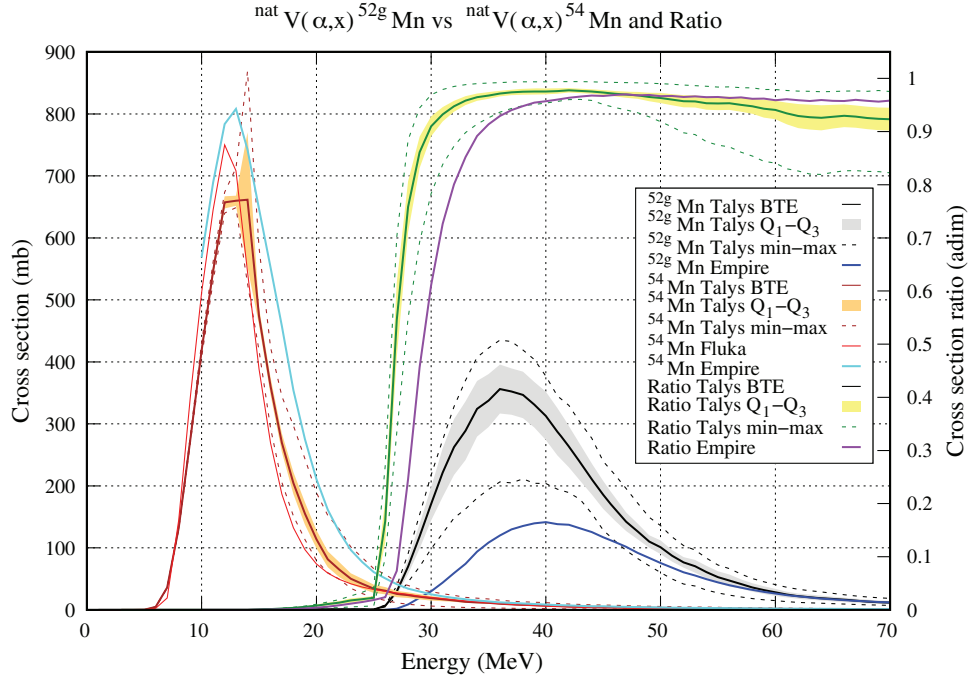
Fig. 2. – Comparison between the theoretical cross sections of ^{52g}Mn (right peak) and ^{54}Mn (left peak) for the ^{nat}V case. The ratio r between the cross section of ^{52g}Mn and its sum with ^{54}Mn is plotted with respect to the right vertical axis. The energy window corresponding to high purity ^{52g}Mn production is clearly visible ($r \simeq 1$).

ref. [15] for a thorough discussion which compares theory and experiment for both ^{54}Mn and ^{52g}Mn. For the former a good agreement between the theoretical curves and the data was found, while for ^{52g}Mn a significant spread of the data was exhibited. Moreover, a different behaviour among the codes was observed with Talys overestimating and Empire underestimating the data.

Following the previously described criterion, from fig. 2 it is possible to identify the energy range (48–33.9 MeV) in which ^{52g}Mn is produced with large cross section while that of ^{54}Mn is very low, as clearly visible also thanks to the cross section ratio shown in the same figure. The comparison between ^{52g}Mn and its contaminants is considered for each reaction in a similar way, properly selecting the energy windows that are reported in table III.

TABLE III. – *Selected energy windows for the considered production routes.*

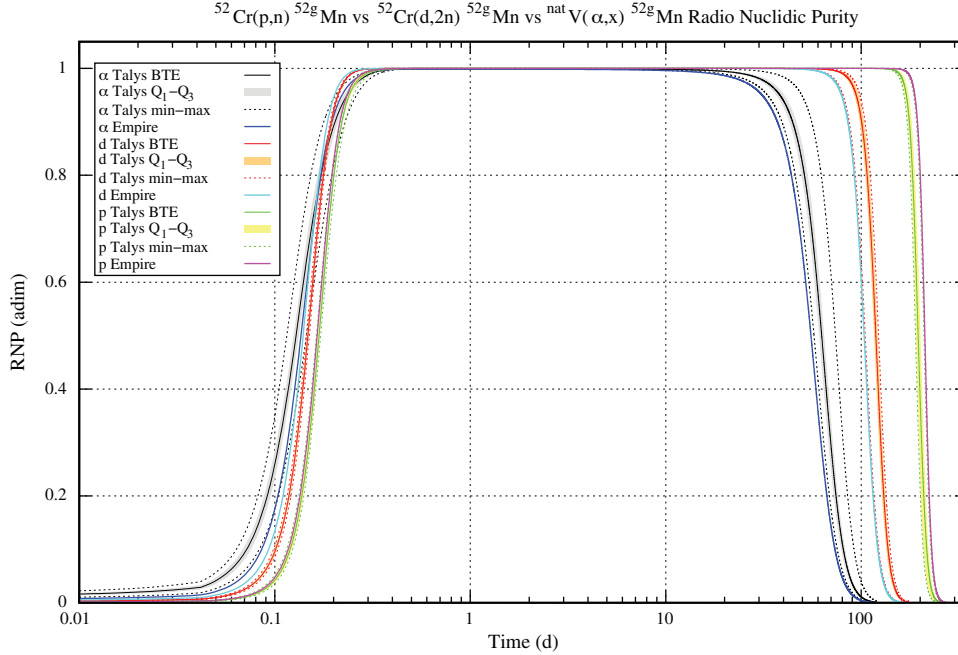| Projectile	Target	Energy window
Protons	^{nat}Cr	17–14 MeV
Protons	^{52}Cr	17–14 MeV
Deuterons	^{52}Cr	20–15.5 MeV
Alpha particles	^{nat}V	48–33.9 MeV

Fig. 3. – Comparison of RNP curves between the reaction with enriched ^{52}Cr and with ^{nat}V.

High levels of radionuclidic purity are very important for clinical applications. We compare this quantity among the reactions with ^{nat}V and with enriched ^{52}Cr in fig. 3 with logarithmic time axis. The reaction with protons has a RNP higher than the other two reactions, since in its energy window ^{52g}Mn is produced with no ^{54}Mn, while the other two reactions produce also ^{54}Mn. The reaction with ^{nat}V produces also the stable ^{55}Mn which nevertheless does not affect the RNP and, in addition, produces a higher quantity of ^{54}Mn which suppresses the RNP at longer times in comparison with the other channels. In the reaction with deuterons the main contaminant is produced via an electromagnetic reaction, and, therefore, its cross section is very low. In fig. 4 we compare the reactions with ^{nat}Cr and ^{nat}V and we show that in the case of ^{nat}V the RNP is higher for longer times, indicating a clear advantage of ^{nat}V with respect to ^{nat}Cr.

However to quantify the amount of ^{52g}Mn produced it is necessary to consider the integral yield of these reactions. In particular the difference of the yields in the selected energy windows is calculated with the BTE curve and with an uncertainty provided by the width of the interquartile band [15]. In fig. 5 the comparison between the integral yields of ^{nat}V and ^{nat}Cr is shown, where the green shaded areas indicate the selected energy windows, referring to 200 μm thick targets. In table IV the yields are reported for all the considered reactions, comparing the codes with Radionuclide Yield Calculator [17] as well as with the available experimental data [18, 19], which are linearly fitted for all reactions. The evaluation obtained with Talys and Empire shows some differences and specifically Empire is close to the data in the reactions with natural targets, while Talys reproduces both the IAEA recommended values and the data for the other two reactions on enriched targets. For ^{nat}Cr targets, it was noted in ref. [15] that a rescaling of the Empire results would show a good agreement with Talys and the data. For the reaction with ^{nat}V targets, Talys estimates a higher value of the integral yield in comparison to the data.
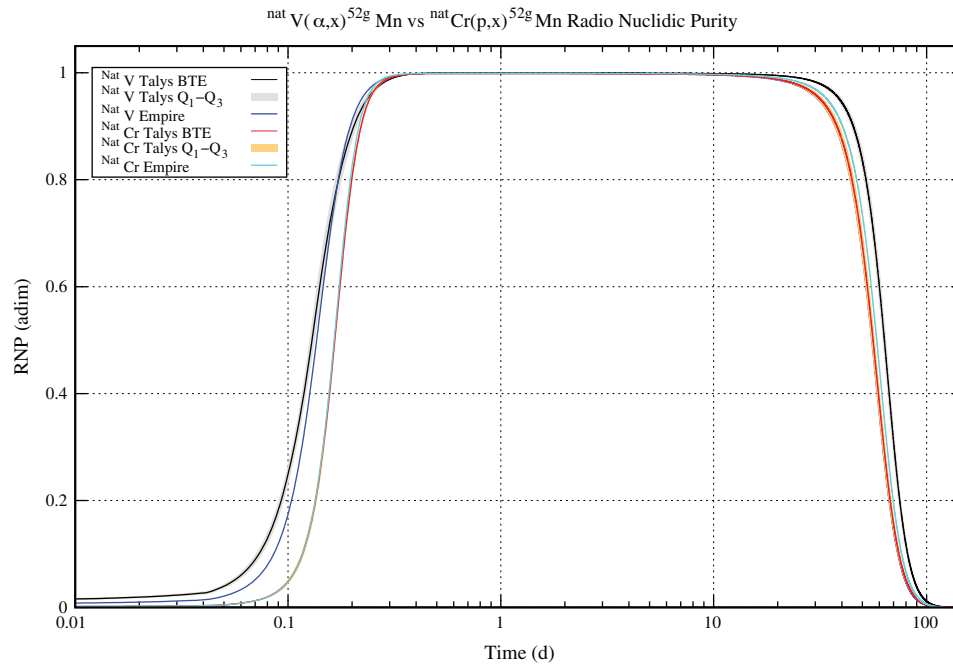
^{nat}V(α,x)^{52g}Mn vs ^{nat}Cr(p,x)^{52g}Mn Radio Nuclidic Purity

Fig. 4. – Comparison of the RNP curves between the reactions with natural targets.

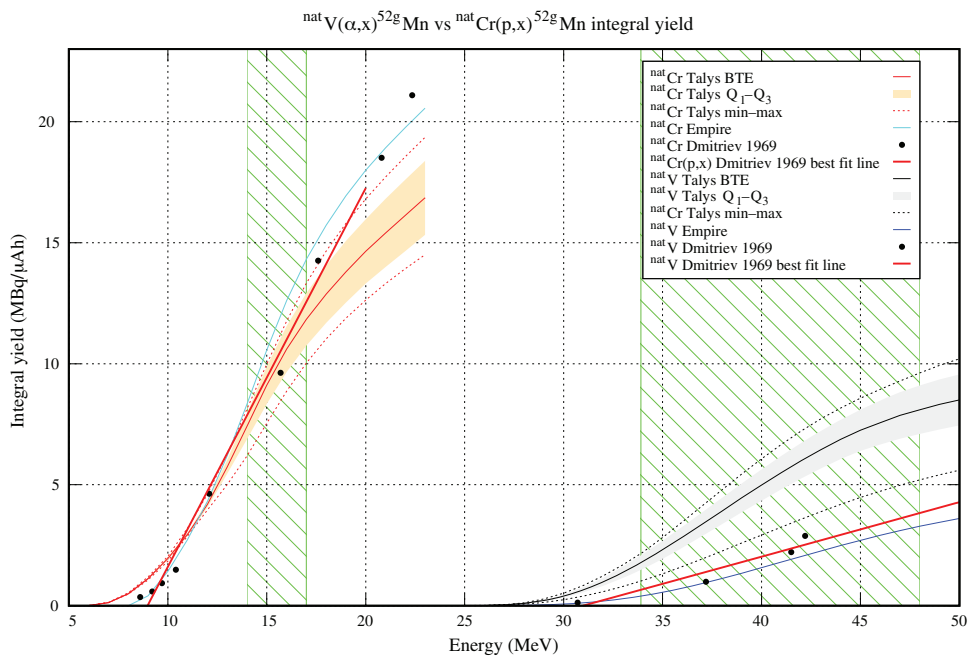^{nat}V(α,x)^{52g}Mn vs ^{nat}Cr(p,x)^{52g}Mn integral yield

Fig. 5. – Comparison of the integral yields between the reactions with natural targets. The yields are calculated with $1\,\mu$A current and $1\,$h of target irradiation. The green shaded area indicates the optimized energy window used for the $200\,\mu$m thick targets.

TABLE IV. – *Comparison of the integral yields for the four production routes analyzed in this work considering irradiation parameters corresponding to $1\,\mu A$ current and $1\,h$ irradiation time. The optimized energy windows for each route, shown in the left column, correspond to a $200\,\mu m$ target thickness. We report Talys calculations with a theoretical error evaluation depending on the variability of the models.*

Reaction [E_i-E_o] (MeV)	Yield: $y(E_i) - y(E_o)$ (MBq/μAh)			
	Talys	Empire	RYC	Data fit or interpolation
^{nat}V(α,x)^{52g}Mn [48-33.9]	6.28 ± 1.27	2.88	5.57	3.17 [18]
^{nat}Cr(p,x)^{52g}Mn [17-14]	4.41 ± 0.51	5.98	4.28	5.52 [18]
^{52}Cr(p,n)^{52g}Mn [17-14]	6.64 ± 1.73	7.06	4.75	6.47 [19]
^{52}Cr(d,2n)^{52g}Mn [20-15.5]	12.00 ± 0.63	10.09	14.43	12.14 [19]

4. – Conclusions

We have investigated different routes for the production of ^{52g}Mn for the innovative PET-MRI MultiModal Imaging technique. In this work the reaction with alpha particles on ^{nat}V has been studied and compared with the standard production routes of ^{52g}Mn, using different nuclear reaction codes (Talys, Fluka and Empire) and considering, in particular, the theoretical variability of the Talys models.

The reaction with ^{nat}V represents a very promising channel with high RNP and yield comparable with the reactions with ^{nat}Cr targets. Specifically this route shows better results in terms of purities and yields if compared with the reaction with ^{nat}Cr, due to a lower production of the contaminants, in particular of ^{54}Mn. Furthermore this reaction, which is based on a natural target, could represent a promising alternative to the reactions with enriched ^{52}Cr, for which specific technologies for the target recovery are required. As shown in ref. [15] new experimental data are needed for a more precise assessment of this promising production route.

* * *

REFERENCES

[1] MARTÍ-BONMATÍ L. *et al.*, *Contrast Media Mol. Imaging*, **5** (2010) 180.
[2] VAIDYANATHAN S. *et al.*, *Clin. Radiol.*, **70** (2015) 787.
[3] MARIANI G. *et al.*, *Eur. J. Nucl. Med. Mol. Imaging*, **37** (2010) 1959.
[4] FRAUM T. J. *et al.*, *Acad. Radiol.*, **23** (2016) 220.
[5] NAZIR M. S. *et al.*, *Eur. Heart J. Cardiovasc. Imaging*, **19** (2018) 962.
[6] MUZIC R. F. jr. and DIFILIPPO F. P., *Semin. Roentgenol.*, **49** (2014) 242.
[7] QAIM S. M., *Medical Radionuclide Production: Science and Technology* (De Gruyter) 2020.
[8] GORIELY S., HILAIRE S. and KONING A. J., *Astron. Astrophys.*, **487** (2008) 767.

[9] HERMAN M. *et al.*, *Nucl. Data Sheets*, **108** (2007) 2655.

[10] BATTISTONI G. *et al.*, in *AIP Conf. Proc.*, **896** (2006) 31.

[11] BARBARO F. *et al.*, these proceedings.

[12] CARANTE M. P. *et al.*, LNL Annual Report 2019, INFN-LNL Report 259 (2020), ISSN 1828-8561.

[13] CANTON L. and FONTANA A., *Eur. Phys. J. Plus*, **135** (2020) 770.

[14] LEO W. R., *Techniques for Nuclear and Particle Physics Experiments* (Springer) 1994.

[15] COLOMBI A. *et al.*, in preparation.

[16] OTUKA N. *et al.*, *Nucl. Data Sheets*, **120** (2014) 272.

[17] SITARZ M. *et al.*, *Instruments*, **3** (2019) 7.

[18] DMITRIEV P. P. *et al.*, *At. Energy*, **26** (1969) 539.

[19] INTERNATIONAL ATOMIC ENERGY AGENCY-NUCLEAR, data services, 2007, `https://www-nds.iaea.org/relnsd/vcharthtml/MEDVChart.html`.